Minimal tight-binding model for the distinct magnetic orders of semihydrogenated and semifluorinated graphene

Lei Hao[1] and C. S. Ting[2]

[1]*Key Laboratory of Quantum Materials and Devices of Ministry of Education, School of Physics, Southeast University, Nanjing 211189, China*
[2]*Texas Center for Superconductivity and Department of Physics, University of Houston, Houston, Texas 77204, USA*

(Received 5 September 2023; revised 9 November 2023; accepted 14 November 2023; published 7 December 2023)

Semihydrogenated graphene (C_2H) and semifluorinated graphene (C_2F), both in the chair conformation, were predicted by first-principles calculations to be ferromagnetic and antiferromagnetic. It is unclear what is the underlying mechanism leading to such distinct magnetic orders of the two materials. We show that a single-orbital tight-binding model of the graphene lattice up to the next-nearest-neighbor hopping term, with one carbon sublattice coupled to a single active orbital of the adatoms (hydrogen for C_2H, and fluorine for C_2F), supplemented by the Hubbard interactions on the carbon sites, correctly reproduces the distinct magnetic orders of C_2H and C_2F. In terms of a fairly good approximation to the low-energy band of the nonmagnetic state, we analytically elucidate how a finite next-nearest-neighbor hopping term makes the bandwidth of the low-energy band of C_2H much smaller than that of C_2F. Competition between the reduction of the interaction energy and the increase of the band energy then favors the ferromagnetic state for C_2H and the antiferromagnetic state for C_2F. Implications of the mechanism, including electric field tuning of the bandwidth and application to elemental analogs of graphene such as silicene, are analyzed.

DOI: 10.1103/PhysRevB.108.245120

I. INTRODUCTION

Functionalization with adatoms provides a very versatile approach of modulating the electronic properties of graphene. By controlling the species, the concentration, and the spatial arrangements of the adatoms, a large variety of functionalized graphene with interesting properties have been studied both theoretically and experimentally [1–18].

Among the vast possibilities explored in the literature, two semifunctionalized graphene, C_2H and C_2F in the chair conformation (defined below), are of special interest. First, they are periodic lattices and have the smallest unit cell among all possible periodic functionalized graphene. As a result, they have well-defined bulk properties compared to nonperiodic functionalized samples, and they are usually easier to prepare experimentally than periodic structures with larger unit cells [19–22]. Second, unlike the fully functionalized graphene that also have a small unit cell but are nonmagnetic insulators [6–9], C_2H and C_2F have been predicted by first-principles calculations to have ferromagnetic and antiferromagnetic ground states [23–30], respectively. As intrinsic two-dimensional (2D) magnets, they may have plenty of applications in spintronics and electronics [23,24].

The mechanism leading to such distinct magnetic tendencies of the two structurally identical materials is still far from clear. The purpose of this work is to identify the underlying mechanism by considering the minimal tight-binding description of the magnetic orders of the two materials.

Compared to first-principles calculations, the tight-binding models are more computationally efficient, and it is easier to obtain a clear physical picture from them for various physical properties. Tight-binding models including only one p_z orbital on each carbon atom, and hopping terms between neighboring sites have successfully accounted for a vast majority of the low-energy properties of graphene [31]. Similar tight-binding models supplemented by coupling with the outer shell orbitals of the adatoms have also been proposed and used to study the properties of functionalized graphene [27–29,32]. For example, many works consider minimal tight-binding models with only nearest-neighbor (NN) hopping terms among the carbon atoms and adatoms [28,33–36].

It is unknown whether such a minimal tight-binding model with only NN hopping terms can account for the distinct magnetic orders (ferromagnetic for C_2H, versus antiferromagnetic for C_2F) of half-filled C_2H and C_2F. Here we show that it is of crucial importance to retain the next-nearest-neighbor (2NN) hopping term to robustly reproduce the distinct magnetic orders of C_2H and C_2F. We show that, with a realistic nonzero 2NN hopping term, the ferromagnetic order of C_2H and antiferromagnetic order of C_2F are robust against the variations of the model parameters related to the adatoms. The reason, as we will clarify, is that the 2NN hopping term together with the opposite on-site energies of hydrogen for C_2H and fluorine for C_2F lead to a much narrower low-energy band for C_2H than that for C_2F. The implications of the mechanism, such as a quasiflat band in C_2H under a perpendicular electric field and related effects in semifunctionalized 2D elemental analogs of graphene, are also discussed.

II. MAGNETIC ORDERS AND THE MINIMAL MODEL

In the chair conformation of C_2H and C_2F that we focus on, the lattice sites belonging to one sublattice (taken as the A sublattice) of the graphene lattice are all functionalized, whereas

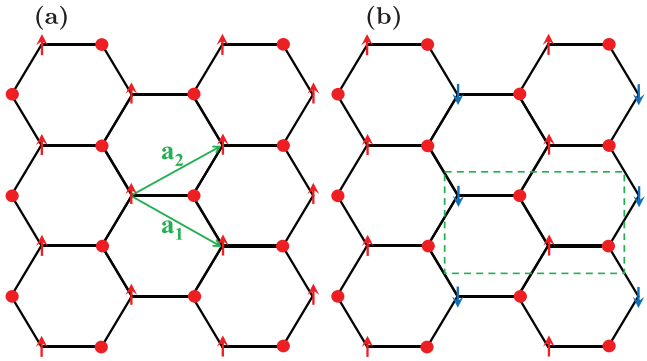

FIG. 1. Top view of the lattices (in the chair conformation) and magnetic orders of (a) C_2H and (b) C_2F. All the A sublattice sites (below the round dots) of the graphene lattice have an adatom (denoted as a round dot) chemisorbed on the top. The B sublattice sites are not functionalized and contribute most significantly to the magnetism. The upward or downward arrow on a B sublattice site represents the orientation of the magnetic moment on this site. The arrangements of the unshown minor magnetic moments on the A sublattice sites and the adatoms follow the same pattern as that shown for the B sublattice sites. In the ferromagnetic state of C_2H, as in the nonmagnetic state of both C_2H and C_2F, the unit cell is the parallelogram subtended by the two primitive lattice vectors, $\mathbf{a}_1 = (\frac{\sqrt{3}}{2}, -\frac{1}{2})a$ and $\mathbf{a}_2 = (\frac{\sqrt{3}}{2}, \frac{1}{2})a$. In the antiferromagnetic state of C_2F, the unit cell is taken as the part encircled by the dashed rectangle, which is subtended by the primitive lattice vectors $\mathbf{v}_1 = (\sqrt{3}, 0)a$ and $\mathbf{v}_2 = (0, 1)a$.

the sites of the other sublattice (the B sublattice) are all unfunctionalized. In the nonmagnetic state, the unit cell consists of two carbon atoms and one adatom, where each adatom chemisorbs a carbon site of the A sublattice at the top position. Figures 1(a) and 1(b) show separately the ferromagnetic and antiferromagnetic orders predicted for C_2H and C_2F by first-principles calculations [23,24]. The antiferromagnetic order of Fig. 1(b) may be called collinear-like antiferromagnetic, due to its apparent similarity to the collinear antiferromagnetic order of LaOFeAs and $BaFe_2As_2$ [37,38]. Since the unfunctionalized carbon sites have the largest moment and contribute most significantly to the magnetism, we plot only the moments on these unfunctionalized B sublattice sites. The minor magnetic moments of the A sublattice sites and the adatoms also follow the same pattern as the B sublattice sites, even though their spin orientations may be different.

The fact that structurally identical C_2H and C_2F develop qualitatively distinct magnetic tendencies is quite interesting. It is unknown whether there is a simple physical picture that underlies this qualitative distinction between the two materials. Tight-binding models have been very successful in explaining and predicting various properties of graphene [31]. Tight-binding models have also been used to study the functionalized graphene [27–29,32,36]. It is unknown what is the minimal tight-binding description for the distinct magnetic orders of C_2H and C_2F.

We consider a minimal tight-binding model with a single orbital on each site of the lattice. The model, $H = H_0 + H_1$, contains the band part H_0 and the interaction part H_1. The band part of the model is

$$H_0 = -t_1 \sum_{\langle i,j\rangle\sigma} (c^\dagger_{i\sigma} c_{j\sigma} + \text{H.c.}) - t_2 \sum_{\langle\langle i,j\rangle\rangle\sigma} (c^\dagger_{i\sigma} c_{j\sigma} + \text{H.c.}) + \epsilon_d \sum_{m\sigma} d^\dagger_{m\sigma} d_{m\sigma} + T \sum_{\langle m,i\rangle\sigma} (d^\dagger_{m\sigma} c_{i\sigma} + \text{H.c.}). \quad (1)$$

$-t_1$ and $-t_2$ are the hopping integrals for the NN and 2NN hopping terms of the graphene lattice. ϵ_d represents the difference between the on-site energy of the adatom orbital and the on-site energy of the carbon p_z orbital (taken as zero). T is the hopping integral between a carbon site of the A sublattice and the adatom above it. H.c. denotes the Hermitian conjugate of the term explicitly written out. $\sigma = \uparrow$ or $\downarrow$ denotes the electron spin.

For H_1, we consider the on-site Hubbard interaction on the carbon atoms,

$$H_1 = U \sum_{i\alpha} \left(\hat{n}_{i\alpha\uparrow} - \frac{1}{2}\right)\left(\hat{n}_{i\alpha\downarrow} - \frac{1}{2}\right). \quad (2)$$

U is the strength of the Hubbard interaction. The summation over i runs over all unit cells of the lattice, and α runs over the A and B sublattices. $\hat{n}_{i\alpha\sigma}$ is the number operator for the electron in the ith unit cell, α sublattice, and σ spin.

Tight-binding models of this kind have been proposed to study the low-energy properties of functionalized graphene. Many authors considered the model with $t_2 = 0$ [28,33–36]. The main purpose of this work is to point out and explain the crucial importance of the 2NN hopping term in accommodating the distinct magnetic orders of C_2H and C_2F. As we clarify in what follows, an unexpected synergistic effect between the 2NN hopping term and the energy difference term causes significant differences in the band structures of C_2H and C_2F. A nonzero third-nearest-neighbor (3NN) hopping term, on the other hand, does not change the qualitative results and can be neglected in the minimal model. We emphasize that, while the tight-binding parameters are empirical, they have well-accepted estimated ranges that can provide decent fitting to the low-energy part of the first-principles band structures [33,34,39], and they have been used successfully to explain or predict a great variety of experimental properties of graphene materials [31–36,39].

For the NN hopping among the carbon sites, we will take $t_1 = 2.6$ eV [33]. For the 2NN hopping term, we will take $t_2 = 0.19$ eV, following the ratio of t_2/t_1 proposed by Hancock and coauthors [39]. As we will show below, changing t_2 to a sightly different value does not change the conclusion of the following analysis. For C_2H, $\epsilon_d = 3$ eV and $T = 6.5$ eV were used by Gmitra and coauthors [33]. We have not found explicit estimations of ϵ_d and T for C_2F. Fluorine is known to be the most electronegative element and form a strong covalent bond with carbon [34], so we are certain to have $\epsilon_d < 0$ and a large T. From the estimated parameters of Irmer and coauthors for the cases of dilute fluorination (e.g., $T = 6.1$ eV and $\epsilon_d = -3.3$ eV for $C_{98}F$) [34], it is reasonable to expect that the T and $|\epsilon_d|$ for C_2F should be no less than those for C_2H. A special set of parameter, which is very convenient for revealing the difference between C_2F and C_2H, is by setting $T = 6.5$ eV and $\epsilon_d = -3$ eV for C_2F, which are separately

equal and opposite to that for C_2H. We will use this parameter set to clarify the difference between the two materials and the significance of a nonzero t_2. Afterwards, we show that the conclusions are robust against variations of the parameters.

Introducing the spin operator $\mathbf{S}^{(i\alpha)} = \frac{1}{2}\sum_{\sigma\sigma'} c^{\dagger}_{i\alpha\sigma}(\boldsymbol{\sigma})_{\sigma\sigma'}c_{i\alpha\sigma'}$, where we set $\hbar = 1$ for simplicity, the Hubbard interaction may be written as

$$H_1 = -2U\sum_{i\alpha} S_z^{(i\alpha)}S_z^{(i\alpha)} + \frac{N}{4}U. \tag{3}$$

$\boldsymbol{\sigma} = (\sigma_1, \sigma_2, \sigma_3)$, σ_i $(i = 1, 2, 3)$ are the Pauli matrices. N is the number of unit cells contained in the lattice, in the nonmagnetic state. i runs over the N unit cells. $\alpha = a$ or b represents the two carbon sublattices. Discarding the constant term $\frac{NU}{4}$, and making the mean-field decoupling, we have

$$H_1 \simeq -2U\sum_{i\alpha}\left(2\left\langle S_z^{(i\alpha)}\right\rangle S_z^{(i\alpha)} - \left\langle S_z^{(i\alpha)}\right\rangle^2\right). \tag{4}$$

The ferromagnetic order of Fig. 1(a) corresponds to $\langle S_z^{(i\alpha)}\rangle = S_z^{(\alpha)}$, independent of the index i. The antiferromagnetic order of Fig. 1(b) found for C_2F by Li and coauthors may be modeled by a spatially modulated order parameter [24]

$$\left\langle S_z^{(i\alpha)}\right\rangle = S_z^{(\alpha)}\cos(\mathbf{Q}\cdot\mathbf{R}_i), \tag{5}$$

where $\mathbf{R}_i$ is the coordinate of the ith unit cell, and the modulation vector $\mathbf{Q} = (1, 0)Q$ with $Q = \frac{2\pi}{\sqrt{3}a}$.

III. MEAN-FIELD RESULTS OF THE MAGNETIC ORDER

We study the mean-field solutions for the half-filled C_2H and C_2F at zero temperature. For a semifunctionalized graphene with N unit cells (i.e., N formula units of C_2H or C_2F) in the nonmagnetic state, there are $3N$ electrons in the system, which stands as a constraint in making the self-consistent calculations for the mean-field parameters [32]. For both C_2H and C_2F, we consider the ferromagnetic and antiferromagnetic solutions defined in Fig. 1 in parallel. The state with lower energy is then identified as the mean-field ground state.

We fix $t_1 = 2.6$ eV, first set $(T, \epsilon_d) = (6.5$ eV, 3 eV) for C_2H and $(T, \epsilon_d) = (6.5$ eV, -3 eV) for C_2F, and study the dependence of the mean-field results on t_2. The convergence in the self-consistent calculations is attained when the changes in all four mean-field parameters $n_{\alpha\sigma}$ $(\alpha = a, b; \sigma = \uparrow, \downarrow)$ are smaller than 10^{-6} [32].

There is no solid consensus on the value of the Hubbard interaction U. Values ranging from as low as 2.1 eV [40] to about 10 eV [41,42] can be found in the literature. It is, however, generally recognized that while the correlation effect is not strong enough to induce symmetry breaking transitions in pristine graphene, it easily introduces magnetic order to the rich variants of graphene (i.e., in the presence of defects, vacancies, edges, etc.) [43–46]. Also, it is well known that the self-consistent mean-field method tends to overestimate the correlation effect and the ordering tendency [47,48]. Overall, we should consider U of medium values, such as between about 3 to about 6 eV, as realistic in our self-consistent mean-field analysis.

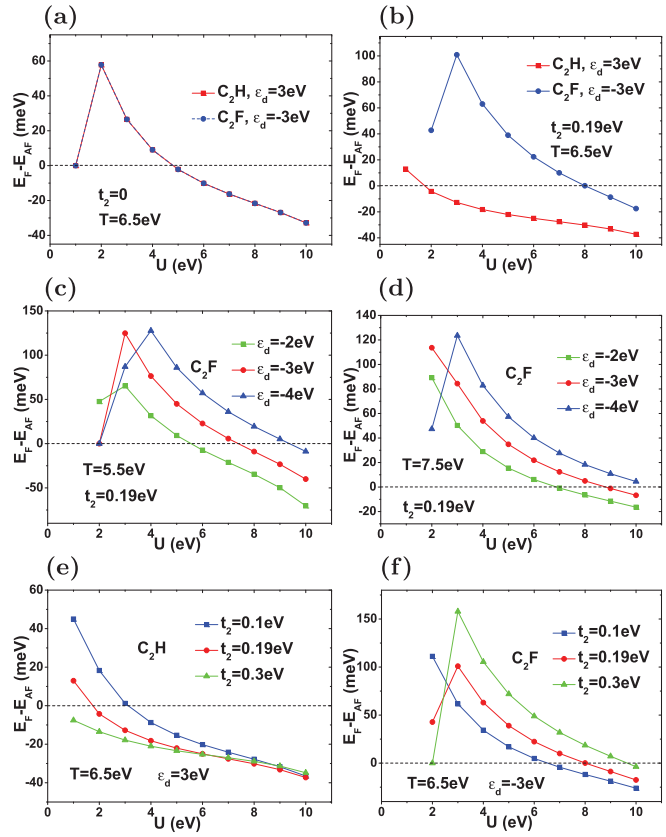

FIG. 2. Differences between the mean-field energies E_F (for the ferromagnetic state) and E_{AF} (for the antiferromagnetic state), per formula unit (containing one carbon atom of the A sublattice, one carbon atom of the B sublattice, and one adatom), as a function of the interaction strength U. $E_F - E_{AF} < 0$ $(E_F - E_{AF} > 0)$ means the ferromagnetic (antiferromagnetic) state has lower energy, for the corresponding parameter combinations shown on the figures. Cases with $E_F - E_{AF} = 0$ for $U = 1$ or 2 eV correspond to nonmagnetic solutions. $t_1 = 2.6$ eV is fixed in all calculations. Other parameters are as shown in the figures.

When we set $t_2 = 0$, as shown in Fig. 2(a), C_2F and C_2H have the same ground state for all interaction strength, although they have opposite ϵ_d. When we set $t_2 = 0.19$ eV, as shown in Fig. 2(b), C_2H and C_2F separately stabilize to the ferromagnetic state and the antiferromagnetic state for a wide range of U, roughly between 2 and 8 eV. As shown in Figs. 2(c) and 2(d), the qualitative conclusion, namely that C_2H and C_2F separately stabilize to the ferromagnetic state and the antiferromagnetic state for medium values of U, is robust to the variations in T and ϵ_d for C_2F. From Figs. 2(e) and 2(f), the conclusion is also robust to the variation of t_2. Overall, the tight-binding model defined by Eqs. (1) and (2) with a finite 2NN hopping term correctly captures the distinct magnetic tendencies of C_2F and C_2H.

IV. MICROSCOPIC MECHANISM IN TERMS OF THE NONMAGNETIC BAND STRUCTURES

In this section, we elucidate the mechanism by which a finite 2NN hopping term separately stabilizes the ferromagnetic state of C_2H and the antiferromagnetic state of C_2F. It turns

out that the 2NN hopping term together with the opposite on-site energies of hydrogen and fluorine make the bandwidth of the low-energy band of C_2H smaller than that of C_2F. The distinct magnetic orders of the two materials are then understood in terms of a competition between the reduction in the interaction energy and the increase in the band energy. Then, we construct an approximate model for the low-energy band. The low-energy band is half-filled in the nonmagnetic state and is crucial to the magnetic transition. In terms of the approximate model, we clarify analytically how a finite t_2 makes the bandwidth of the low-energy bands of the two materials different. In light of the analytical analysis, we make conjectures on the physical implications of the mechanism on C_2H, C_2F, and several 2D elemental analogs of graphene with a honeycomb lattice.

A. Nonmagnetic band structures

The band structures in the nonmagnetic state are determined by H_0. Introducing the basis $\psi^\dagger_{\mathbf{k}\sigma} = [d^\dagger_{\mathbf{k}\sigma}, a^\dagger_{\mathbf{k}\sigma}, b^\dagger_{\mathbf{k}\sigma}]$, where $d^\dagger_{\mathbf{k}\sigma}$, $a^\dagger_{\mathbf{k}\sigma}$, and $b^\dagger_{\mathbf{k}\sigma}$ are separately the creation operators for the orbitals on the adatom, the A sublattice site, and the B sublattice site, we can write

$$H_0 = \sum_{\mathbf{k}\sigma} \psi^\dagger_{\mathbf{k}\sigma} h_0(\mathbf{k}) \psi_{\mathbf{k}\sigma}. \tag{6}$$

The model Hamiltonian $h_0(\mathbf{k})$ is a 3×3 matrix

$$h_0(\mathbf{k}) = \begin{pmatrix} \epsilon_d & T & 0 \\ T & \xi_2(\mathbf{k}) & \xi_1(\mathbf{k}) \\ 0 & \xi_1^*(\mathbf{k}) & \xi_2(\mathbf{k}) \end{pmatrix}, \tag{7}$$

where

$$\xi_1(\mathbf{k}) = -t_1(e^{i\mathbf{k}\cdot\boldsymbol{\delta}_1} + e^{i\mathbf{k}\cdot\boldsymbol{\delta}_2} + e^{i\mathbf{k}\cdot\boldsymbol{\delta}_3}), \tag{8}$$

$$\xi_2(\mathbf{k}) = -2t_2[\cos(\mathbf{k}\cdot\mathbf{a}_1) + \cos(\mathbf{k}\cdot\mathbf{a}_2) + \cos(\mathbf{k}\cdot\mathbf{a}_3)]. \tag{9}$$

The new vectors in the above definitions are $\boldsymbol{\delta}_1 = (-1, 0)a_0$, $\boldsymbol{\delta}_2 = (\frac{1}{2}, -\frac{\sqrt{3}}{2})a_0$, $\boldsymbol{\delta}_3 = (\frac{1}{2}, \frac{\sqrt{3}}{2})a_0$, and $\mathbf{a}_3 = \mathbf{a}_2 - \mathbf{a}_1 = (0, 1)a$. $a_0 = a/\sqrt{3}$ is the length of the NN carbon bond.

The eigenspectrum of Eq. (7) is exactly solvable. Shown in Fig. 3 are the band structures of the noninteracting C_2H and C_2F for $t_2 = 0$ and $t_2 = 0.19$ eV. We have taken $T = 6.5$ eV. ϵ_d for C_2H and C_2F are separately taken as 3 and -3 eV. For $t_2 = 0$, as shown in Figs. 3(a) and 3(b), the bandwidths of the low-energy middle band for C_2H and C_2F are identical. In the presence of a small $t_2 = 0.19$ eV, as shown in Figs. 3(c) and 3(d), the bandwidth of the middle band of C_2H (C_2F) is suppressed (increased). The contrast in the bandwidth of the low-energy band for $t_2 = 0.19$ eV is more clear in Figs. 3(e) and 3(f). Changing slightly the value of t_2 or the values of T and ϵ_d for C_2F does not change the notable differences between the bandwidths of the low-energy bands of C_2H and C_2F.

B. Correlation between band structures and magnetic order

For the half-filled systems that we focus on, the middle band of the nonmagnetic band structures is half-filled and is the low-energy band. The properties of the middle band are of crucial importance to the magnetic tendency of the system at finite U.

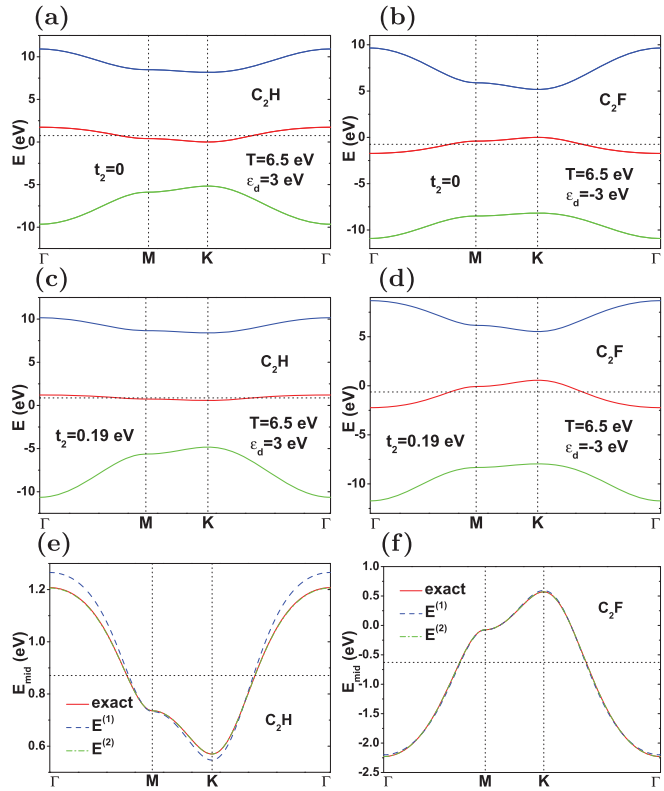

FIG. 3. Band structures of C_2H and C_2F in the nonmagnetic state for $U = 0$. Parts (a) and (b) are for zero 2NN hopping, $t_2 = 0$. Parts (c) and (d) are for a nonzero 2NN hopping, $t_2 = 0.19$ eV. Part (e) [(f)] shows the exact and approximate dispersions for the low-energy middle band of (c) [(d)]. The approximate dispersions, $E^{(1)}$ and $E^{(2)}$, are defined in Sec. IV C. The horizontal dotted line in each figure lies at the Fermi level. The high symmetry points of the 2D Brillouin zone (BZ) are $\boldsymbol{\Gamma} = (0, 0)$, $\mathbf{M} = (1, 0)\frac{2\pi}{\sqrt{3}a}$, and $\mathbf{K} = (\frac{\sqrt{3}}{2}, \frac{1}{2})\frac{4\pi}{3a}$.

In itinerant magnetism, the ferromagnetic state stabilizes by minimizing the on-site Coulomb repulsion between opposite-spin electrons, at the expense of an increase in the band energy [49]. So, the ferromagnetic state is usually favored in narrow bands, because the minimization of the interaction energy easily outweighs the increase of the band energy. If the band is not narrow enough, the system may make a compromise between the reduction of the interaction energy and the gain of the band energy by forming the antiferromagnetic state. Comparing the mean-field results of Fig. 2(b) and the band structures of Figs. 3(c) and 3(d), this picture seems to account for the distinct magnetic tendencies of C_2H and C_2F.

To check whether the above general picture is applicable to the present problem, we have calculated the band part (E_{band}) and the interaction part (E_{int}) of the total energy, which are separately defined as the average of H_0 of Eq. (1) and H_1 of Eq. (4) with respect to the mean-field state. The interaction part is simply

$$E_{\text{int}} = -2U\left[\left(S_z^{(a)}\right)^2 + \left(S_z^{(b)}\right)^2\right]. \tag{10}$$

Since $|S_z^{(b)}| \gg |S_z^{(a)}|$, and the low-energy band contains most of the weight of the p_z orbital of the B sublattice, the low-energy band accounts for most of the reduction of the interaction energy.

The band part of the model may be written generally as

$$H_0 = \sum_{\mathbf{k}\alpha\beta} c^\dagger_{\mathbf{k}\alpha} h_{\alpha\beta}(\mathbf{k}) c_{\mathbf{k}\beta}, \tag{11}$$

where the wave vector $\mathbf{k}$ runs over the BZ, and α and β run over the spin and orbital degrees of freedom of the unit cell. E_{band} is defined as

$$\begin{aligned} NE_{\text{band}} &= \langle 0|H_0|0\rangle \\ &= \sum_{\mathbf{k}\alpha\beta,\gamma} h_{\alpha\beta}(\mathbf{k}) U^*_{\alpha\gamma}(\mathbf{k}) U_{\beta\gamma}(\mathbf{k}) \theta(E_F - E_\gamma(\mathbf{k})) \\ &= N_{\text{uc}} \sum_\gamma E^{(\gamma)}_{\text{band}}. \end{aligned} \tag{12}$$

N is the number of formula units (each of which has a carbon atom of the A sublattice, a carbon atom of the B sublattice, and an adatom) in the lattice, N_{uc} is the number of unit cells. $N = N_{\text{uc}}$ for the ferromagnetic state, and $N = 2N_{\text{uc}}$ for the antiferromagnetic state. $|0\rangle$ is the mean-field state obtained by the self-consistent calculation. $E_\gamma(\mathbf{k})$ is the γth eigenstate of the mean-field Hamiltonian, whose eigenvector is stored in the γth column of the unitary matrix $U(\mathbf{k})$. $\gamma = 1, 2, \ldots, 6$ ($\gamma = 1, 2, \ldots, 12$) for the ferromagnetic (the antiferromagnetic) state. The eigenvalues increase with the index γ. E_F is the Fermi level in the mean-field band structures, determined by the constraint that the lowest $3N$ mean-field states are occupied. $\theta(x)$, which is the Heaviside function, is 1 for $x > 0$ and 0 otherwise.

In the nonmagnetic state, the low-energy middle band is half-filled and the lowest band is fully occupied. It is interesting to compare the separate contributions of these two bands to E_{band}. For this purpose, we define $E^{(\text{middle})}_{\text{band}}$ and $E^{(\text{low})}_{\text{band}}$ to represent the contributions of the middle band and the lowest band. For the ferromagnetic state, we have $E^{(\text{middle})}_{\text{band}} = E^{(3)}_{\text{band}}$ and $E^{(\text{low})}_{\text{band}} = E^{(1)}_{\text{band}} + E^{(2)}_{\text{band}}$. For the antiferromagnetic state, we have $E^{(\text{middle})}_{\text{band}} = (E^{(5)}_{\text{band}} + E^{(6)}_{\text{band}})/2$ and $E^{(\text{low})}_{\text{band}} = (E^{(1)}_{\text{band}} + E^{(2)}_{\text{band}} + E^{(3)}_{\text{band}} + E^{(4)}_{\text{band}})/2$.

As shown in Fig. 4(a), the stabilization of the ferromagnetic state for C_2H is dominated by the lowering of the interaction energy. The band energy, as shown in Fig. 4(c), comes as a compensation between $E^{(\text{middle})}_{\text{band}}$ and $E^{(\text{low})}_{\text{band}}$. On the other hand, for medium U, E_{band} follows the trend of $E^{(\text{middle})}_{\text{band}}$ more closely. So, together with the dominance of the middle band in the interaction energy, the middle band plays the most important role in stabilizing the ferromagnetic state of C_2H.

From Fig. 4(b), the antiferromagnetic state stabilizes for C_2F because of the smaller increase in the band energy than that for the ferromagnetic state. From Fig. 4(d), it is clear that the larger increase of the band energy of the ferromagnetic state for medium U comes from the contribution of the middle band. So again, the middle band plays the most important role in stabilizing the antiferromagnetic state of C_2F.

Overall, the magnetic orders of C_2H and C_2F may be understood from the competition between the interaction energy and the band energy. The low-energy middle band of the nonmagnetic band structures plays the decisive role in leading to the distinct magnetic orders of the two materials. The 2NN hopping term, which is responsible for the significant difference between the bandwidths of the low-energy bands of the two materials, is therefore of crucial importance for the distinct magnetic orders of C_2H and C_2F.

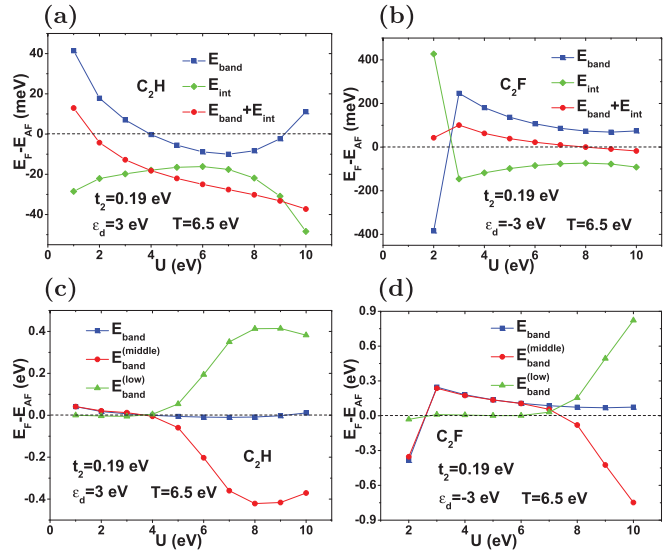

FIG. 4. (a) C_2H and (b) C_2F, differences in the band part (E_{band}), interaction part (E_{int}), and the total mean-field ground-state energy ($E_{\text{band}} + E_{\text{int}}$), between the ferromagnetic state and the antiferromagnetic state. In (b) at $U = 2$ eV, the antiferromagnetic state is already stabilized but the ferromagnetic initial state still leads to a nonmagnetic state, which explains why the results of E_{band} and E_{int} for $U = 2$ eV show different behavior compared to those for larger U. (c) C_2H and (d) C_2F, contributions of the lowest-energy band [$E^{(\text{low})}_{\text{band}}$] and the middle band [$E^{(\text{middle})}_{\text{band}}$] to E_{band}.

C. Analytical analysis of the bandwidth of the low-energy band based on an approximate dispersion

It is well known that the 2NN hopping term breaks the particle-hole symmetry of the graphene band structures [31]. We would like to clarify how the 2NN hopping term together with the opposite signs of the ϵ_d parameters for C_2H and C_2F lead to the striking difference in the bandwidths of their low-energy bands.

The three-orbital model of Eq. (7) for the nonmagnetic state is exactly solvable. The exact results, however, are cumbersome for analytical analysis. An approximate dispersion for the low-energy band that is both simple enough and also sufficiently accurate is therefore highly desirable. Such an approximation is possible because the low-energy band is associated mainly with the p_z orbital of the unfunctionalized B sublattice carbon sites. This is not only verified from explicit calculation of the density of states, but also physically transparent since the strong covalent bonds between the p_z orbital of the A sublattice sites and the adatom orbital turn these orbitals into high-energy levels. As a result, we may construct an approximation centering around the unchemisorbed carbon

orbital, and taking the influences of the other two orbitals into account.

By projecting the 3×3 model of Eq. (7) to the subspace of the B sublattice [50,51], we get the following expression for the dispersion of the low-energy band:

$$E = \xi_2(\mathbf{k}) + \frac{|\xi_1(\mathbf{k})|^2(E-\epsilon_d)}{(E-\epsilon_d)[E-\xi_2(\mathbf{k})]-T^2}. \tag{13}$$

The first term on the right-hand side of the equation arises from the coupling among the B sublattice sites through the 2NN hopping. The second term arises from the coupling of the B sublattice sites with the A sublattice sites and the adatoms through the NN hopping terms. Equation (13) defines an iteration function for the dispersion of the low-energy band. However, this iteration function does not saturate as the iteration number increases, possibly because the energy appears in the denominator.

Equation (13) may be adapted to the following equation:

$$E = \frac{(E-\epsilon_d)(E-\xi_2)^2 + T^2\xi_2 + |\xi_1|^2\epsilon_d}{T^2+|\xi_1|^2}. \tag{14}$$

We have suppressed the $\mathbf{k}$-dependence of $\xi_1(\mathbf{k})$ and $\xi_2(\mathbf{k})$. Again, Eq. (14) defines an iterative relation. Since the energy of the carbon p_z orbital has been taken as zero, the lowest-order approximation to Eq. (14) follows by setting the energy $E = E^{(0)} = 0$ on the right-hand side of Eq. (14), which gives

$$E^{(1)} = \frac{\epsilon_d|\xi_1|^2 + \xi_2(T^2-\xi_2\epsilon_d)}{T^2+|\xi_1|^2}. \tag{15}$$

Substituting $E = E^{(1)}$ to the right-hand side of Eq. (14) gives $E^{(2)}$, and so on. As shown in Figs. 3(e) and 3(f), $E^{(1)}$ already provides a fairly good approximation to the low-energy bands of Figs. 3(c) and 3(d). $E^{(2)}$ is almost indistinguishable from the exact results. While higher-order iterations give better and better approximations, we will use the simplest $E^{(1)}$ to analytically study the influences of t_2 on the bandwidth of the low-energy band.

To begin the analysis, notice that $E^{(1)}(\mathbf{k})$ depends on the wave vector through a combination $f(\mathbf{k})$ defined as

$$f(\mathbf{k}) = \cos(\mathbf{k}\cdot\mathbf{a}_1) + \cos(\mathbf{k}\cdot\mathbf{a}_2) + \cos(\mathbf{k}\cdot\mathbf{a}_3), \tag{16}$$

because

$$\xi_2(\mathbf{k}) = -2t_2 f(\mathbf{k}), \tag{17}$$

$$|\xi_1(\mathbf{k})|^2 = 3t^2 + 2t^2 f(\mathbf{k}). \tag{18}$$

Therefore, we can write

$$E^{(1)}(\mathbf{k}) = \frac{Af^2+Bf+C}{Df+D'}, \tag{19}$$

where the constants are defined as

$$\begin{aligned} A &= -4\epsilon_d t_2^2, \\ B &= 2\left(\epsilon_d t_1^2 - t_2 T^2\right), \\ C &= 3\epsilon_d t_1^2, \\ D &= 2t_1^2, \\ D' &= T^2 + 3t_1^2. \end{aligned} \tag{20}$$

The function $f(\mathbf{k})$ has its maximum 3 at the center (i.e., the $\mathbf{\Gamma}$ point) of the BZ. It can be shown that $f(\mathbf{k})$ attains its minimum $-\frac{3}{2}$ at the $\mathbf{K}$ points of the BZ.

From Fig. 3, the dispersion of the low-energy band is monotonic in the range of $f \in [-\frac{3}{2}, 3]$ for both $t_2 = 0$ and $t_2 = 0.19$ eV. In terms of $E^{(1)}(\mathbf{k})$, we determine the range of t_2 for which the low-energy band is monotonic in $f \in [-\frac{3}{2}, 3]$. To judge the monotonicity of $E^{(1)}$, we study its derivative with respect to f,

$$\frac{dE^{(1)}}{df} = \frac{ADf^2 + 2AD'f + BD' - CD}{(Df+D')^2}. \tag{21}$$

Since the denominator is positive definite in $f \in [-\frac{3}{2}, 3]$, the monotonicity of $E^{(1)}$ is determined by the numerator of the right-hand side of Eq. (21), which we define as

$$(Df+D')^2\frac{dE^{(1)}}{df} = G(f). \tag{22}$$

For $t_2 = 0$, $G(f)$ is a constant. The derivative, therefore, has the same sign in the range $f \in [-\frac{3}{2}, 3]$, so that the maximum and minimum of the band are attained among $\mathbf{K}$ and $\mathbf{\Gamma}$. For $t_2 > 0$, $G(f)$ is a quadratic function with a vertex at

$$-\frac{D'}{D} = -\frac{3}{2} - \frac{T^2}{2t_1^2} < -\frac{3}{2}. \tag{23}$$

Therefore, $G(f)$ is monotonic in the range of $f \in [-\frac{3}{2}, 3]$. If $G(f)$ has the same sign at $f = -\frac{3}{2}$ and 3, $E^{(1)}$ is monotonic in $f \in [-\frac{3}{2}, 3]$.

For $\epsilon_d > 0$, which is relevant to C_2H, we have $G(f = -\frac{3}{2}) = G(f = 3) > 0$ for $t_2 = 0$. As we increase $t_2 > 0$, we have $G(f = -\frac{3}{2}) > G(f = 3)$, and $G(f = 3)$ decreases. So, the critical t_2 beyond which $E^{(1)}$ is nonmonotonic in $f \in [-\frac{3}{2}, 3]$ is determined by $G(f = 3) = 0$, which gives t_{2c}, the critical value of t_2, as

$$\frac{\sqrt{\left(3t_1^2+T^2\right)^2T^4 + 48\epsilon_d^2t_1^2T^2\left(6t_1^2+T^2\right)} - \left(3t_1^2+T^2\right)T^2}{24\epsilon_d\left(6t_1^2+T^2\right)}. \tag{24}$$

For $0 \leqslant t_2 \leqslant t_{2c}$, $G(f) \geqslant 0$ in $f \in [-\frac{3}{2}, 3]$. Correspondingly, $E^{(1)}$ is a monotonically increasing function in $f \in [-\frac{3}{2}, 3]$, attaining its minimum at $f = -\frac{3}{2}$ (i.e., at $\mathbf{K}$) and maximum at $f = 3$ (i.e., at $\mathbf{\Gamma}$). For $(t_1, T, \epsilon_d) = (2.6\text{ eV}, 6.5\text{ eV}, 3\text{ eV})$, we have $t_{2c} \simeq 0.252$ eV.

For $\epsilon_d < 0$, which is relevant to C_2F, we have $G(f = -\frac{3}{2}) = G(f = 3) < 0$ for $t_2 = 0$. As we increase $t_2 > 0$, we have $G(f = -\frac{3}{2}) < G(f = 3)$ and $G(f = 3)$ increases. Again, the critical t_2 beyond which $E^{(1)}$ is nonmonotonic in $f \in [-\frac{3}{2}, 3]$ is determined by $G(f = 3) = 0$, which gives the critical value of t_2 in this case, t'_{2c}, as

$$\frac{\sqrt{\left(3t_1^2+T^2\right)^2T^4 + 48\epsilon_d^2t_1^2T^2\left(6t_1^2+T^2\right)} + \left(3t_1^2+T^2\right)T^2}{-24\epsilon_d\left(6t_1^2+T^2\right)}. \tag{25}$$

For $0 \leqslant t_2 \leqslant t'_{2c}$, $G(f) \leqslant 0$ in $f \in [-\frac{3}{2}, 3]$. Correspondingly, $E^{(1)}$ is a monotonically decreasing function in

$f \in [-\frac{3}{2}, 3]$, attaining its maximum at $f = -\frac{3}{2}$ (i.e., at **K**) and minimum at $f = 3$ (i.e., at **Γ**). For $(t_1, T, \epsilon_d) = (2.6\text{ eV}, 6.5\text{ eV}, -3\text{ eV})$, we have $t'_{2c} \simeq 1.139$ eV.

Since clearly $t_{2c} < t'_{2c}$, we will focus on the parameter ranges of $0 < t_2 < t_{2c}$, which is wide enough to include the physically relevant cases. Note that, for $t_2 \leqslant t_{2c}$, the exact dispersions of the low-energy bands of C_2H and C_2F are indeed both monotonic in $f \in [-\frac{3}{2}, 3]$. For slightly larger t_2 (e.g., $t_2 = 0.3$ eV), the low-energy band of C_2H is no longer monotonic in $f \in [-\frac{3}{2}, 3]$. However, the large contrast in the bandwidths of the low-energy bands of the two materials remains, and the qualitative tendency of the magnetic order, namely that C_2H and C_2F separately favor the ferromagnetic and antiferromagnetic states, is still correct.

According to the above analysis, for $0 < t_2 \leqslant t_{2c}$, the approximate dispersion of the low-energy band always takes its maximal and minimal values at the end points of the section $f \in [-\frac{3}{2}, 3]$, which are

$$E^{(1)}\left(f = -\frac{3}{2}\right) = 3t_2 - \frac{9t_2^2}{T^2}\epsilon_d,$$
$$E^{(1)}(f = 3) = -\frac{6T^2}{T^2 + 9t_1^2}t_2 + \frac{9(t_1^2 - 4t_2^2)}{T^2 + 9t_1^2}\epsilon_d. \quad (26)$$

The bandwidth is simply

$$\Delta = |E^{(1)}(f = -\tfrac{3}{2}) - E^{(1)}(f = 3)|. \quad (27)$$

For $t_2 = 0$, the bandwidth is independent of the sign of ϵ_d. For $0 < t_2 \leqslant t_{2c}$, and also for $t_2 < t_1/2$, which is obeyed by all realistic considerations, reversing the sign of ϵ_d clearly changes the bandwidth. Explicitly, fixing the amplitudes of all parameters, with $0 < t_2 \leqslant t_{2c}$, positive ϵ_d relevant to C_2H gives a bandwidth smaller than that given by negative ϵ_d relevant to C_2F. Also notice that for realistic model parameters, the coefficients of t_2 in Eqs. (26) and (27) have magnitudes larger than 1, whereas the coefficients of ϵ_d have magnitudes smaller than 1. This character enhances the significance of the 2NN hopping term, compared to that of the energy difference term, in determining the bandwidth of the low-energy band, and it explains why a small t_2 can make the bandwidth of the low-energy band of C_2H much smaller than that of C_2F.

The above results may be applied to the bandwidths of the spin-split low-energy bands in the ferromagnetic state. Considering a fixed set of hopping parameters (including a finite t_2), the bandwidth of the low-energy band depends on ϵ_d, which is the difference between the on-site energy of the adatom orbital and the p_z orbital of the unchemisorbed B sublattice sites. In the ferromagnetic state, the mean-field decoupling of Eq. (4) to the Hubbard interaction introduces an additional spin-resolved on-site energy to the B sublattice orbitals. For the ferromagnetic solutions of C_2H and C_2F, the additional on-site energy for the lower spin-split band is $-2U|\langle S_z^{(b)}\rangle|$. This changes the energy difference from ϵ_d to $\epsilon_d + 2U|\langle S_z^{(b)}\rangle|$. For C_2H with $\epsilon_d = 3$ eV, the mean-field correction enhances the difference of the on-site energies, which tends to increase the bandwidth of the lower spin-split band. Since this mechanism is less effective in the antiferromagnetic state, because there are two B sublattice sites with opposite spin orientations in the unit cell, we see that the band energy of the lower spin-split low-energy band of the ferromagnetic state tends to decrease compared to that of the antiferromagnetic state [see $E_{\text{band}}^{(\text{middle})}$ in Fig. 4(c)], and therefore it also helps to stabilize the ferromagnetic state in C_2H. For C_2F with $\epsilon_d = -3$ eV, the correction has the opposite sign, which tends to decrease the bandwidth of the lower spin-split band for medium U. This provides another angle to see why the ferromagnetic state is disfavored in C_2F.

D. Immediate implications of the mechanism

The above analysis immediately leads to two interesting conjectures. First, it is possible to make the low-energy band of C_2H narrower by tuning ϵ_d through a perpendicular electric field. For fixed $(t_1, t_2, T) = (2.6\text{ eV}, 0.19\text{ eV}, 6.5\text{ eV})$, and ignoring the difference in the on-site energies of the A and B sublattices resulting from the perpendicular electric field, the bandwidth is reduced if we decrease ϵ_d from 3 eV. For $\epsilon_d = 3$ eV, as shown in Fig. 3(e), the low-energy band has a bandwidth of about 637.5 meV. This bandwidth may be reduced to about 12.9 meV for $\epsilon_d \simeq 1.8175$ eV. The order-of-magnitude reduction in the bandwidth of the low-energy band greatly enhances the correlation effect. It is intriguing to explore possible correlated phases with novel topological order in C_2H with reduced bandwidth [52–55] if the spin-orbit coupling is considered [10–12,33–36]. The tight-binding theory could also be used to study the interplay of superconductivity and the magnetic order in the doped C_2H and C_2F due to the Hubbard interaction U by the method of random phase approximations [56,57]. These topics will constitute our subjects for future study.

Second, it might be possible to tune C_2H and C_2F close to or even cross the phase transition point between the ferromagnetic state and the antiferromagnetic state. For C_2F, this is achieved by reducing the bandwidth of the low-energy middle band by increasing ϵ_d (i.e., decreasing $-\epsilon_d = |\epsilon_d|$) with a perpendicular electric field. For C_2H, this is achieved by increasing the bandwidth of the low-energy band by increasing $\epsilon_d > 0$ with a perpendicular electric field.

As another implication, we notice that there are 2D elemental analogs of graphene, including silicene [58–63], germanene [64–66], and stanene [67,68], which all have honeycomb structures that are usually buckled. While the structural buckling makes the physics more complicated than graphene, it has been proved that similar single-orbital tight-binding model may be used to describe the low-energy properties of these 2D graphene analogs [69]. When considering the semihydrogenation or semifluorination of these materials [70–72], we suspect that similar physics should play a role. First, in full analogy to the semifunctionalized graphene, a finite 2NN hopping term together with the energy difference term can lead to significant differences in the bandwidths of the low-energy bands of semihydrogenated and semifluorinated graphene analog materials, which may induce distinct magnetic tendencies in them. There have been studies on the semihydrogenated graphene analog materials, which commonly find ferromagnetic semiconducting states [72–75]. The magnetic properties of semifluorinated graphene analog materials are less explored. In a study by Wu *et al.* [76], stanene and germanene

semifunctionalized by iodine are found to show ferromagnetic order, but stanene and germanene semifunctionalized by bromine or chlorine are found to show antiferromagnetic order. Following this trend, it seems reasonable to expect an antiferromagnetic tendency in semifluorinated graphene analog materials. Second, electric field tuning of the bandwidth should also be active in semihydrogenated and semifluorinated graphene analog materials. Compared to the flat graphene lattice, pristine graphene analog materials have a buckled structure, and functionalization tends to enhance the buckling [72–75]. Due to the buckling of the structure, a perpendicular electric field can induce a tunable band gap in the band structures of pristine graphene analog materials [59,60,66]. For the semifunctionalized graphene analog materials in a perpendicular electric field, two effects of comparable significance should play a role. The first effect is an energy difference between the adatom orbital and the orbital of the underlying pristine lattice. As with the semifunctionalized graphene, this effect tends to change the bandwidth of the low-energy band. The second effect is an energy difference between the two sublattices of the underlying lattice. While this effect is also present in the semifunctionalized graphene, it is more important and non-negligible in the semifunctionalized graphene analog materials with much larger structural buckling. The interplay of these two effects, and their impacts on the magnetic behaviors and other properties of semifunctionalized graphene analog materials, are intriguing subjects for future studies.

V. SUMMARY

To consistently account for the ferromagnetic order of C_2H and the antiferromagnetic order of C_2F, as we have illustrated, it is crucial to consider a tight-binding model including the 2NN hopping term among the carbon orbitals. The combination of this term with the opposite on-site energies of the adatoms for C_2H and C_2F leads to significantly different bandwidths of the low-energy bands of the two materials, which in turn accounts for their different magnetic tendencies. The minimal tight-binding model, together with the mean-field magnetic orders consistent with first-principles results, may facilitate further studies of fundamental and application-related properties of C_2H and C_2F. The implications of the mechanism clarified, such as electric field tuning of the bandwidths and possible relevancy to several 2D elemental analogs of graphene, are interesting topics for future studies.

ACKNOWLEDGMENTS

The research of C.S.T. was supported by the Texas Center for Superconductivity at the University of Houston and by the Robert A. Welch Foundation.

[1] B. Uchoa, V. N. Kotov, N. M. R. Peres, and A. H. Castro Neto, Phys. Rev. Lett. **101**, 026805 (2008).
[2] K. T. Chan, J. B. Neaton, and M. L. Cohen, Phys. Rev. B **77**, 235430 (2008).
[3] M. Wu, E.-Z. Liu, and J. Z. Jiang, Appl. Phys. Lett. **93**, 082504 (2008).
[4] H. Johll, H. C. Kang, and E. S. Tok, Phys. Rev. B **79**, 245416 (2009).
[5] A. H. Castro Neto and F. Guinea, Phys. Rev. Lett. **103**, 026804 (2009).
[6] J. O. Sofo, A. S. Chaudhari, and G. D. Barber, Phys. Rev. B **75**, 153401 (2007).
[7] D. C. Elias, R. R. Nair, T. M. G. Mohiuddin, S. V. Morozov, P. Blake, M. P. Halsall, A. C. Ferrari, D. W. Boukhvalov, M. I. Katsnelson, A. K. Geim, and K. S. Novoselov, Science **323**, 610 (2009).
[8] H. Şahin, M. Topsakal, and S. Ciraci, Phys. Rev. B **83**, 115432 (2011).
[9] S. Li, J. Li, Y. Wang, C. Yu, Y. Li, W. Duan, Y. Wang, and J. Zhang, Nat. Electron. **4**, 254 (2021).
[10] J. Ding, Z. Qiao, W. Feng, Y. Yao, and Q. Niu, Phys. Rev. B **84**, 195444 (2011).
[11] C. Weeks, J. Hu, J. Alicea, M. Franz, and R. Wu, Phys. Rev. X **1**, 021001 (2011).
[12] H. Zhang, C. Lazo, S. Blügel, S. Heinze, and Y. Mokrousov, Phys. Rev. Lett. **108**, 056802 (2012).
[13] M. Neek-Amal and F. M. Peeters, Phys. Rev. B **92**, 155430 (2015).
[14] H.-C. Huang, S.-Y. Lin, C.-L. Wu, and M.-F. Lin, Carbon **103**, 84 (2016).
[15] K. E. Whitener Jr., J. Vac. Sci. Technol. A **36**, 05G401 (2018).
[16] S. Wellnhofer, A. Stabile, D. Kochan, M. Gmitra, Y.-W. Chuang, J. Zhu, and J. Fabian, Phys. Rev. B **100**, 035421 (2019).
[17] Z. Jiang, W. Lou, Y. Liu, Y. Li, H. Song, K. Chang, W. Duan, and S. Zhang, Phys. Rev. Lett. **124**, 166401 (2020).
[18] S. Cao, C. Cao, S. Tian, and J.-H. Chen, Phys. Rev. B **102**, 045402 (2020); **104**, 125422 (2021).
[19] H.-Y. Lu, L. Hao, R. Wang, and C. S. Ting, Phys. Rev. B **93**, 241410(R) (2016).
[20] H.-Y. Lu, A. S. Cuamba, S.-Y. Lin, L. Hao, R. Wang, H. Li, Y. Y. Zhao, and C. S. Ting, Phys. Rev. B **94**, 195423 (2016).
[21] H.-Y. Lu, A. S. Cuamba, L. Geng, L. Hao, Y.-M. Qi, and C. S. Ting, Phys. Rev. B **96**, 165420 (2017).
[22] H. Chen, D.-L. Bao, D. Wang, Y. Que, W. Xiao, G. Qian, H. Guo, J. Sun, Y.-Y. Zhang, S. Du, S. T. Pantelides, and H.-J. Gao, Adv. Mater. **30**, 1801838 (2018).
[23] J. Zhou, Q. Wang, Q. Sun, X. S. Chen, Y. Kawazoe, and P. Jena, Nano Lett. **9**, 3867 (2009).
[24] L. Li, R. Qin, H. Li, L. Yu, Q. Liu, G. Luo, Z. Gao, and J. Lu, ACS Nano **5**, 2601 (2011).
[25] L. Feng and W. X. Zhang, AIP Adv. **2**, 042138 (2012).
[26] D. W. Boukhvalov, Phys. E **43**, 199 (2010).
[27] A. N. Rudenko, F. J. Keil, M. I. Katsnelson, and A. I. Lichtenstein, Phys. Rev. B **88**, 081405(R) (2013).
[28] K. Seki, T. Shirakawa, Q. Zhang, T. Li, and S. Yunoki, Phys. Rev. B **93**, 155419 (2016).
[29] V. V. Mazurenko, A. N. Rudenko, S. A. Nikolaev, D. S. Medvedeva, A. I. Lichtenstein, and M. I. Katsnelson, Phys. Rev. B **94**, 214411 (2016).

[30] W. Zhao, J. Gebhardt, F. Späth, K. Gotterbarm, C. Gleichweit, H.-P. Steinrück, A. Görling, and C. Papp, Chem. A Eur. J. **21**, 3347 (2015).

[31] A. H. Castro Neto, F. Guinea, N. M. R. Peres, K. S. Novoselov, and A. K. Geim, Rev. Mod. Phys. **81**, 109 (2009).

[32] L. Hao, H.-Y. Lu, and C. S. Ting, Phys. Rev. Mater. **3**, 024003 (2019).

[33] M. Gmitra, D. Kochan, and J. Fabian, Phys. Rev. Lett. **110**, 246602 (2013).

[34] S. Irmer, T. Frank, S. Putz, M. Gmitra, D. Kochan, and J. Fabian, Phys. Rev. B **91**, 115141 (2015).

[35] D. Kochan, S. Irmer, and J. Fabian, Phys. Rev. B **95**, 165415 (2017).

[36] L. Brey, Phys. Rev. B **92**, 235444 (2015).

[37] C. de la Cruz, Q. Huang, J. W. Lynn, J. Li, W. Ratcliff II, J. L. Zarestky, H. A. Mook, G. F. Chen, J. L. Luo, N. L. Wang, and P. Dai, Nature (London) **453**, 899 (2008).

[38] Q. Huang, Y. Qiu, W. Bao, M. A. Green, J. W. Lynn, Y. C. Gasparovic, T. Wu, G. Wu, and X. H. Chen, Phys. Rev. Lett. **101**, 257003 (2008).

[39] Y. Hancock, A. Uppstu, K. Saloriutta, A. Harju, and M. J. Puska, Phys. Rev. B **81**, 245402 (2010).

[40] J. L. McChesney, A. Bostwick, T. Ohta, T. Seyller, K. Horn, J. González, and E. Rotenberg, Phys. Rev. Lett. **104**, 136803 (2010).

[41] T. O. Wehling, E. Şaşıoğlu, C. Friedrich, A. I. Lichtenstein, M. I. Katsnelson, and S. Blügel, Phys. Rev. Lett. **106**, 236805 (2011).

[42] E. Şaşıoğlu, H. Hadipour, C. Friedrich, S. Blügel, and I. Mertig, Phys. Rev. B **95**, 060408(R) (2017).

[43] M. Fujita, K. Wakabayashi, K. Nakada, and K. Kusakabe, J. Phys. Soc. Jpn. **65**, 1920 (1996).

[44] Y.-W. Son, M. L. Cohen, and S. G. Louie, Phys. Rev. Lett. **97**, 216803 (2006).

[45] E. J. Duplock, M. Scheffler, and P. J. D. Lindan, Phys. Rev. Lett. **92**, 225502 (2004).

[46] H. Hadipour, Phys. Rev. B **99**, 075102 (2019).

[47] S. Sorella and E. Tosatti, Europhys. Lett. **19**, 699 (1992).

[48] L. M. Martelo, M. Dzierzawa, L. Siffert, and D. Baeriswyl, Z. Phys. B **103**, 335 (1996).

[49] S. Blundell, *Magnetism in Condensed Matter* (Oxford University Press, Oxford, 2001).

[50] L. Hao and T. K. Lee, J. Phys.: Condens. Matter **27**, 105701 (2015).

[51] E. McCann and V. I. Fal'ko, Phys. Rev. Lett. **96**, 086805 (2006).

[52] E. J. Bergholtz and Z. Liu, Int. J. Mod. Phys. B **27**, 1330017 (2013).

[53] S. A. Parameswaran, R. Roy, and S. L. Sondhi, C. R. Phys. **14**, 816 (2013).

[54] Z. Liu, F. Liu, and Y.-S. Wu, Chin. Phys. B **23**, 077308 (2014).

[55] O. Derzhko, J. Richter, and M. Maksymenko, Int. J. Mod. Phys. B **29**, 1530007 (2015).

[56] D. J. Scalapino, E. Loh, Jr., and J. E. Hirsch, Phys. Rev. B **34**, 8190(R) (1986).

[57] Z. Y. Weng, T. K. Lee, and C. S. Ting, Phys. Rev. B **38**, 6561 (1988).

[58] G. G. Guzmán-Verri and L. C. Lew Yan Voon, Phys. Rev. B **76**, 075131 (2007).

[59] N. D. Drummond, V. Zólyomi, and V. I. Fal'ko, Phys. Rev. B **85**, 075423 (2012).

[60] Z. Ni, Q. Liu, K. Tang, J. Zheng, J. Zhou, R. Qin, Z. Gao, D. Yu, and J. Lu, Nano Lett. **12**, 113 (2012).

[61] P. Vogt, P. De Padova, C. Quaresima, J. Avila, E. Frantzeskakis, M. C. Asensio, A. Resta, B. Ealet, and G. Le Lay, Phys. Rev. Lett. **108**, 155501 (2012).

[62] B. Feng, Z. Ding, S. Meng, Y. Yao, X. He, P. Cheng, L. Chen, and K. Wu, Nano Lett. **12**, 3507 (2012).

[63] A. Fleurence, R. Friedlein, T. Ozaki, H. Kawai, Y. Wang, and Y. Yamada-Takamura, Phys. Rev. Lett. **108**, 245501 (2012).

[64] M. E. Dávila, L. Xian, S. Cahangirov, A. Rubio, and G. L. Lay, New J. Phys. **16**, 095002 (2014).

[65] L. Li, S.-Z. Lu, J. Pan, Z. Qin, Y.-Q. Wang, Y. Wang, G.-Y. Cao, S. Du, and H.-J. Gao, Adv. Mater. **26**, 4820 (2014).

[66] P. Bampoulis, C. Castenmiller, D. J. Klaassen, J. van Mil, Y. Liu, C.-C. Liu, Y. Yao, M. Ezawa, A. N. Rudenko, and H. J. W. Zandvliet, Phys. Rev. Lett. **130**, 196401 (2023).

[67] F.-F. Zhu, W.-J. Chen, Y. Xu, C.-L. Gao, D.-D. Guan, C.-H. Liu, D. Qian, S.-C. Zhang, and J.-F. Jia, Nat. Mater. **14**, 1020 (2015).

[68] J. Deng, B. Xia, X. Ma, H. Chen, H. Shan, X. Zhai, B. Li, A. Zhao, Y. Xu, W. Duan, S.-C. Zhang, B. Wang, and J. G. Hou, Nat. Mater. **17**, 1081 (2018).

[69] C.-C. Liu, H. Jiang, and Y. Yao, Phys. Rev. B **84**, 195430 (2011).

[70] L. C. Lew Yan Voon, E. Sandberg, R. S. Aga, and A. A. Farajian, Appl. Phys. Lett. **97**, 163114 (2010).

[71] C. Si, J. Liu, Y. Xu, J. Wu, B.-L. Gu, and W. Duan, Phys. Rev. B **89**, 115429 (2014).

[72] C.-W. Zhang and S.-S. Yan, J. Phys. Chem. C **116**, 4163 (2012).

[73] X.-Q. Wang, H.-D. Li, and J.-T. Wang, Phys. Chem. Chem. Phys. **14**, 3031 (2012).

[74] F. Pan, R. Quhe, Q. Ge, J. Zheng, Z. Ni, Y. Wang, Z. Gao, L. Wang, and J. Lu, Phys. E **56**, 43 (2014).

[75] A. Mahmood and G. Rahman, J. Phys.: Condens. Matter **32**, 205501 (2020).

[76] S.-C. Wu, G. Shan, and B. Yan, Phys. Rev. Lett. **113**, 256401 (2014).